A&A manuscript no.
(will be inserted by hand later)

Your thesaurus codes are:
03(03.04.1; 07.09.1; 07.19.1: 09.13.1; 20.01.2)

ASTRONOMY
AND
ASTROPHYSICS
1.2.2008

Extragalactic Large-Scale Structures behind the Southern Milky Way. – I. Redshifts Obtained at the SAAO in the Hydra/Antlia Extension*

R.C. Kraan-Korteweg[1], **A.P. Fairall**[2], **and C. Balkowski**[3]

[1] Kapteyn Astronomical Institute, Postbus 800, 9700 AV Groningen, The Netherlands
[2] Department of Astronomy, University of Cape Town, Rondebosch, 7700 South Africa
[3] Observatoire de Paris, DAEC, Unité associée au CNRS, D0173, et à l'Université Paris 7, 92195 Meudon Cedex, France

Received date;accepted date

Abstract. Spectroscopic observations have been carried out for galaxies in the Milky Way with the 1.9 m telescope of the South African Astronomical Observatory (SAAO). The galaxies were selected from a deep optical galaxy search covering $266° \lesssim \ell \lesssim 296°, |b| \lesssim 10°$ (Kraan-Korteweg 1994). This is in the extension of the Hydra and Antlia clusters *and* in the approximate direction of the dipole anisotropy in the Cosmic Microwave Background radiation.

The galaxies in the SAAO observing program – one of the three complementary approaches in mapping the 3D galaxy distribution in the ZOA – were selected for high central surface brightness and for even distribution over the whole search area. The majority of the galaxies have (absorbed) magnitudes in the range $14\overset{m}{.}5 < B_J < 17\overset{m}{.}5$. Good S/N redshifts were determined for 115 galaxies. One spectrum confirmed a planetary nebula, whereas another object with $v = 57\,km\ sec^{-1}$ most likely is galactic as well. The spectra of the other 25 galaxies either have low S/N or were dominated by superimposed foreground stars.

A preliminary description of the distribution in velocity space is given. We do find evidence for a continuation of the Hydra/Antlia supercluster across the ZOA to $b \approx -10°$, making it one of the larger structures (supercluster?) in the nearby Universe. However, the prominent overdensity unveiled in the galaxy search in Vela ($l \approx 280°, b \approx +6°$) does not, contrary to what may be expected from the 2D distribution, blend with the Hydra and Antlia supercluster ($v \approx 3000\,km\ sec^{-1}$). The latter seems concentrated at $v \approx 6000\,km\ sec^{-1}$. Whether it is related to the Great Attractor cannot yet be assessed. Another weaker concentration is found at $v \approx 9700\,km\ sec^{-1}$. Further out, only tentative conclusions can be made. However, a distinct overabundance of redshifts around $v \approx 16000\,km\ sec^{-1}$ is found, corresponding to that of the adjacent dense Shapley (Alpha) region in the northern galactic hemisphere *and* to that of the Horologium superclusters in the southern galactic hemisphere. This might indicate that these two overdensities are part of a single massive structure, bisected by the Milky Way.

Key words: redshifts of galaxies – clustering of galaxies – zone of avoidance – large-scale structure of the Universe

1. Introduction

1.1. Indications of interesting extragalactic structures in the Southern Milky Way

Some of the nearest and apparently most influential concentrations of galaxies in the sky are largely obscured by the Southern Milky Way ($220° < l < 360°$). Their importance follows from various lines of evidence.

The dipole of the Cosmic Microwave Background (CMB) at $\ell = 264°, b = +48°$ (Kogut *et al.* 1993) implies a motion of our galaxy of $\sim 600\,km\ sec^{-1}$ towards $\ell = 268°, b = +27°$, after the Sun's galactocentric velocity is subtracted and corrections for the motion of our galaxy within the Local Group (LG) have been applied. If an infall of about $v_{vc} = 220\,km\ sec^{-1}$ towards the Virgo cluster (Tammann and Sandage, 1985) is taken into account the direction shifts closer to the Galactic plane ($\ell = 274°, b = +11°$), in the region of the Hydra and Antlia clusters ($270°, +26°$ and $273°, +18°$, respectively). This leads immediately to the question as to whether unknow extragalactic features – which might prove relevant

Send offprint requests to: Renée C. Kraan-Korteweg

* Table 1 is also available in electronic form. See the Editorial in A&AS 1994, Vol. 103, No.1

in explaining the dipole motion – are hidden behind the obscuration layer of our Milky Way.

Such a previously unsuspected overdensity has, for instance, been predicted in the zone of avoidance (ZOA) in Puppis ($l = 245°$), based on an analysis of IRAS galaxies using spherical harmonics by Scharf *et al.* (1992). This overdensity seems to match successfully a nearby cluster identified by one of us through HI-observations of obscured galaxies (Kraan-Korteweg and Huchtmeier 1992). From a subsequent analysis in this area, we concluded that this previously unknown cluster is second only to Virgo in the nearby Universe and adds at least $30\,km\ sec^{-1}$ to the motion of the LG perpendicular to the SGP (Lahav *et al.* 1993).

The peculiar motions of galaxies can be established by comparing redshifts and distances estimated by the Tully-Fisher method for spirals (Aaronson *et al.* 1982) and the modified Faber-Jackson relation for ellipticals (Lynden-Bell *et al.* 1988). Such peculiar motions have revealed large-scale streaming motions towards a "Great Attractor" in the southern sky, close to the galactic plane. An update by Dressler (1991) predicts its center at $\ell = 307°, b = +9°, cz = 4350\,km\ sec^{-1}$, while the most recent density reconstructions from the analysis of the assumed irrotational peculiar velocity field (POTENT) put it even closer to the galactic equator at $\ell \approx 320°, b \approx 0°$ (Kolatt *et al.* 1994).

The existence of this massive overdensity is still quite controversial. Dressler and Faber (1990a,b) find weak evidence for backside infall into the putative Great Attractor, but Mathewson *et al.* (1992) and Hudson (1993,1994) dispute this and claim that no major mass density can be hidden in the ZOA. They, and others, using deep IRAS-redshift surveys and cluster samples (*e.g.*, Rowan-Robinson *et al.* 1990, Scaramella 1991, Lauer and Postman, 1993, Plionis *et al.* 1993), suggest a residual bulk motion caused by much more distant overdensities ($v > 10000\,km\ sec^{-1}$). But this is contradicted with investigations by *e.g.*, Lynden-Bell *et al.* (1989), Strauss *et al.* (1992), and Jerjen and Tammann (1993), who find convergence of the dipole motion between $3500\,km\ sec^{-1}$ to $6500\,km\ sec^{-1}$. Still, it should be noted that this large-scale bulk motion – if real – is also located in the general vicinity of the CMB dipole and the southern Milky Way.

Whatever the case, the mass distribution hidden by the Galactic zone of avoidance appears crucial. This is manifested also with the recent POTENT analysis by Kolatt, Dekel and Lahav (1994), in which they show that the gravitational acceleration at the Local Group changes by 31° when the matter distribution from within $|b| < 20°$ is included, bringing it very close to the CMB dipole.

If mass overdensities are visible as galaxy overdensities (*e.g.*, Dekel, 1994 §6.1) it is important to unveil the distribution of galaxies behind the southern Milky Way - with particular interest in the CMB area ($\ell \approx 275°$) and the Great Attractor region ($\ell \approx 315°$). Such is the purpose of an optical galaxy search started by one of us. It concerns a region of the ZOA, with $266° < \ell < 296°, |b| \lesssim 10°$ (cf. Kraan-Korteweg 1989,1992a,b,1994), *i.e.*, in the close proximity of the CMB dipole. At the time of writing, this survey is being continued in collaboration with Woudt beyond $\ell = 296°$ to $\ell \lesssim 330°$ to cover the "Great Attractor" region (cf. Kraan-Korteweg and Woudt 1994b, for a status report on these surveys).

In order to map the filamentary features and overdensities discovered in 3-dimensional space we have started to measure the redshifts of a representable part of these galaxies. This paper reports on redshift observations made with the 1.9m telescope of the SAAO in the ZOA in the extension of the Hydra and Antlia clusters.

The optical search procedure and the detected galaxy distribution in the Hydra/Antlia region is reviewed in section 1.2. In Section 1.3, our observing strategy in determining the 3-dimensional distribution of these galaxies is outlined. Section 2 then concentrates on the optical spectroscopy of the brighter galaxies in our search area that was done at the SAAO: the observing and reduction procedures are discussed in 2.1, and the resulting recession velocities together with the optical parameters of the observed galaxies are presented in 2.2. This is followed in section 2.3 with a discussion of the properties of the observed galaxy sample, including velocity data for 31 galaxies in our sample region taken from other sources. In the third section we describe the resulting galaxy distribution in redshift space, and discuss the indicated clustering and filamentary structures, in context to known large-scale features adjacent to the zone of avoidance.

1.2. The galaxy search behind the Milky Way in the extension of the Hydra/Antlia clusters

The obscuration of the Milky Way reduces the apparent magnitudes and apparent angular diameters of galaxies (cf. Cameron 1990). For this reason, galaxies which lie close to the galactic plane fail to meet the criteria for inclusion in catalogues (such as *e.g.*, Lauberts 1982) and only few galaxies are known below galactic latitudes of $|b| \lesssim 10°$. Added to this are the enormous numbers of foreground stars that frequently fall on the galaxy images and crowd the field of view. A separation of galaxy and star images cannot as yet be done by automated measuring machines such as COSMOS or APM on a viable basis below $|b| \lesssim 10 - 15°$. Examination by eye is still the best technique, though surveys by eye are clearly both very trying and time consuming and maybe not as objective.

Nevertheless, such a survey has been carried within our region of interest. The tools for this galaxy search are very simple. It comprises a viewer with the ability to magnify 50 times and the IIIaJ film copies of the ESO/SERC survey. Full details about this galaxy search will be presented in the galaxy catalogue which is in preparation (Kraan-Korteweg 1994 [KK94]). The success of the pro-

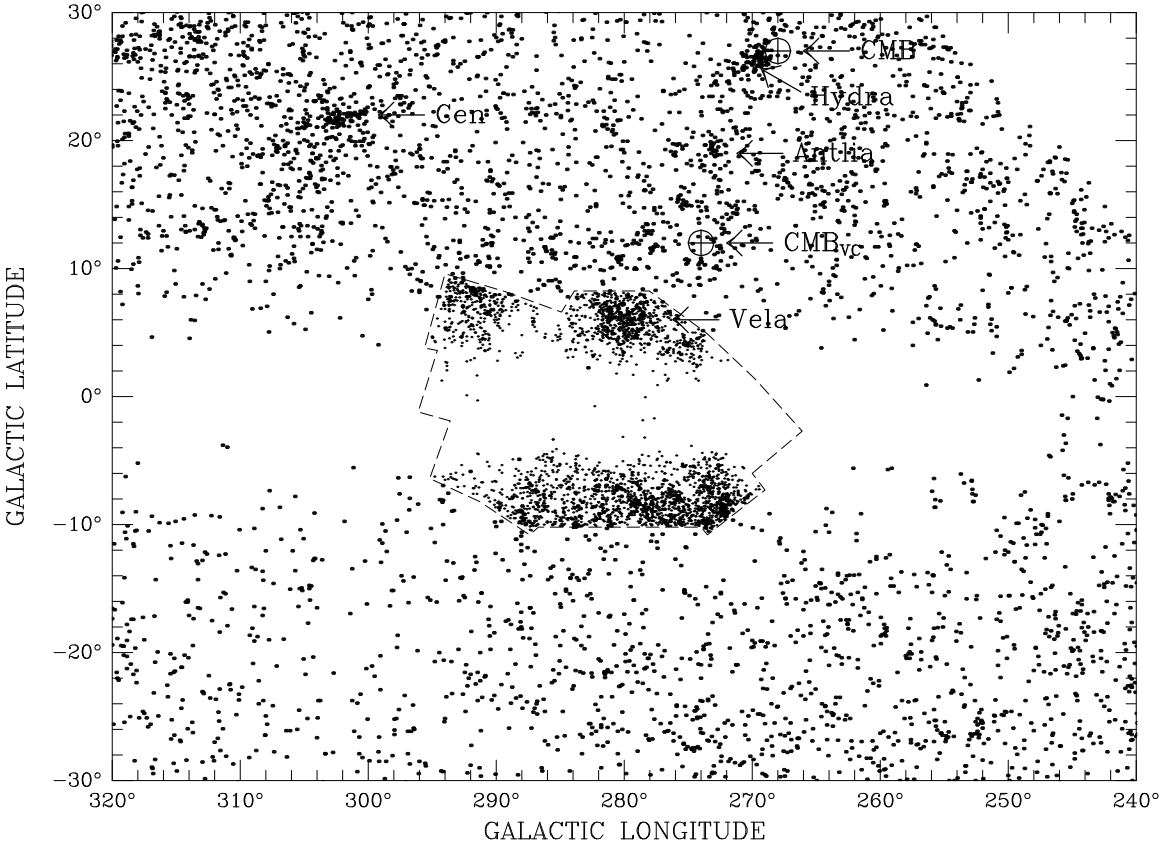

Fig. 1. Distribution of galaxies in the Hydra/Antlia extension. The outlined area marks the area searched in the ZOA. The 3279 galaxies (D$\gtrsim$ 0.′2) unveiled there are shown as small dots. In the surrounding area the Lauberts galaxies are displayed (large dots, D$\geq$ 1.′0). The Hydra, Antlia, Vela and Centaurus clusters are identified, and the CMB-dipole direction, observed (CMB) as well as corrected for virgocentric infall (CMB$_{VC}$ with $v_{VC} = 220\,km\ sec^{-1}$).

cedure for identifying extragalactic objects at very low latitudes is underlined in the present survey, where of the 142 candidates, only three proved to be foreground stars – or were obscured by foreground stars – and only two were found to be galactic nebulae. The main characteristics of this search and the typical properties of the discovered galaxies have been discussed already in earlier work (*e.g.*, Kraan-Korteweg, 1989, 1991, 1992a,b, Kraan-Korteweg and Woudt 1994b) and only the most important aspects will be reviewed here briefly.

The galaxy search in the ZOA in the Hydra/Antlia extension covers the area $266° \lesssim \ell \lesssim 296°$ and $-10° \lesssim b \lesssim +8°$. This region of approximately 400□° encompasses 18 fields of the ESO/SERC survey (F91-F93, F125-F129, F165-F170, F211-F214) and its boundary is outlined in Fig. 1.

A diameter limit of $D \gtrsim 0.'2$ was imposed. Below this diameter the reflection crosses of the stars disappear, making it hard to to differentiate consistently between stars or blended stars and faint galaxies.

In this way 3279 galaxies have been discovered of which only 97 galaxies were previously recorded by Lauberts (1982). The galaxies found in our search are entered as small dots in Fig. 1. It is obvious from the distribution of these newly identified galaxies that the band of obscuration has been narrowed down to $-4° \lesssim b \lesssim 1.°5$. There are even a handfull of galaxies within those limits, suggestive of thinning of the dust layer at $\ell \approx 278°$ and $\ell \approx 293°$. The variation in galaxy density, however, reflects more than obscuration by the Milky Way. There are conspicuous overdensities, foremost around $\ell = 280°, b = +6°$ (the Vela overdensity), $\ell = 275°, b = -9°$ and $\ell = 292°, b = +8°$, indicative of extragalactic large-scale structures present in the survey area.

In order to view the connectivity of these features with their surroundings we have added the galaxies from the ESO Catalogue (Lauberts 1982) to Fig. 1, *i.e.*, all known galaxies with $D \geq 1 arcmin$. The most interesting features are marked, including the CMB dipole direction. The concentration of these galaxies in the top left corner is part of the Centaurus Supercluster with $cz = 4500\,km\ sec^{-1}$ (*e.g.*, Fairall and Jones 1991). Our local (Virgo) Supercluster is an appendage to this dominant structure. At the top, just to the right of the center, a conspicuous filamentary structure extends down towards the Galactic Plane. It includes Hydra ($cz = 3000\,km\ sec^{-1}, \ell = 270°, b = +26°$),

Antlia ($cz = 2800\,km\ sec^{-1}, \ell = 273°, b = 18°$), and the Vela overdensity unveiled in our search. Most of this supercluster complex is visible in Fig. 1. There is also an extension from Centaurus to Pavo ($cz = 4500\,km\ sec^{-1}, \ell = 330°, b = -25°$).

It is obvious from the distribution of ESO-galaxies that a significant portion of the supercluster complex is hidden by the Milky Way but that we can trace these structures much closer to the galactic dust equator with our deep galaxy search. However, the measurement of radial velocities is required to (a) confirm the extragalactic origin of of these overdensities, (b) to map them in three dimensions, and (c) to link them to extragalactic large-scale features above and below the Zone of Avoidance.

1.3. Ongoing observational programs to outline the 3-dimensional galaxy distribution

In collaboration with different groups, various observational programs were started with this goal in mind. The three ongoing approaches so far are multifiber spectroscopy in high density areas, optical spectroscopy of individual galaxies with high central surface brightness (HSB), and HI-observations of low surface brightness (LSB) extended spiral galaxies. The different approaches are complementary with regard to the results they can achieve and the structures they will trace (cf. Kraan-Korteweg *et al.*, 1994a for a discussion on this).

The multifiber spectroscopy is optimal for the high-density areas. These observations are being done at the 3.6m telescope of ESO with Optopus and Mefos. The results are in preparation and will be presented in paper II and III of these series by Cayatte, Balkowski and Kraan-Korteweg. We find that the multifiber spectroscopy – as expected – preferentially picks up condensed clusters. They furthermore allow a glimpse at the galaxy distribution through selected small fields (windows) in the ZOA out to large distances ($v \lesssim 25000\,km\ sec^{-1}$). These observations are therefore also important in outlining structures on very large scales (walls, sheets, etc.).

For determinations of the peculiar velocity of the Local Group (LG) and the mapping of the velocity flow fields, a redshift coverage of the nearby galaxy population – as complete as possible – is essential. This is not straightforward to realise. Because of the thick foreground layer of gas and dust we are seeing only diminished images of the galaxies. Our minimal goal was to observe all the 'brighter' and 'larger' galaxies within our search area, and, in addition, get a fairly homogeneous coverage over the whole search area.

This can be achieved with optical spectroscopy of individual galaxies with a fairly high central surface brightness, i.e. early type galaxies or spirals with a distinct bright bulge. The extremely low surface brightness (LSB) spiral galaxies are mainly late-type galaxies and irregulars, *i.e.*, gas-rich, and can be detected in HI. Together, the methods are well suited in tracing nearby filamentary structures, and complementary in the sense that the optical observations allow redshift determinations of early-type galaxies (which cannot be observed in HI) whilst the 21cm line observations – unaffected by foreground obscuration – allow the detection of the most absorbed LSB spiral galaxies close to the galactic dust equator (which cannot be observed in the optical).

Both methods are being undertaken. The program to observe LSB spiral galaxies is being pursued with the 64m radio telescope at Parkes by Kraan-Korteweg, Henning, Schröder and van Woerden and will be published as paper IV of these series.

Meanwhile, three weeks of observing time with the 1.9m telescope of the SAAO have been devoted to the optical spectroscopy of obscured galaxies, with relatively high central surface brightness. In the allocated period, we observed most galaxies in the survey region from which a reasonable signal-to-noise ratio spectrum could be expected within one hour of exposure time.

2. Observations at the SAAO of Galaxies Selected in the ZOA

2.1. Observing and Reduction Procedures

The spectroscopic observations were made in March and April 1991, and in January 1992, at the South African Astronomical Observatory (SAAO) at Sutherland. We used the 1.9m Radcliffe reflector, with "Unit" spectrograph and reticon photon-counting detector (Jordon *et al.* 1982). The detector has two one-dimensional arrays, each 1872 pixels, set to monitor positions $30''$ apart in the sky: thus one array records the galaxy plus sky while the other measures only the sky. To improve sky subtraction, galaxies were observed on each of the arrays in turn - unless close neighbouring stars made this impossible. All galaxy integrations were bracketed by argon lamp arcs. Maximum time between arcs was $1500sec$ with the telescope near the meridian, and less when aimed well off the meridian and subject to possible flexure in the instrument. In general, the brighter galaxies required only one pair of integrations. For many of the fainter galaxies, multiple pairs of integrations were necessary to yield reasonable S/N spectra, the total integration time sometimes exceeding an hour. The observing routine included exposures of radial-velocity standard stars (mainly during twilight) as well as "flat-fields" at the beginning and end of each night. The dispersion used was approximately $210 \mathring{A}/mm$ (Grating 7), corresponding to $2.8 \mathring{A}$ per pixel. The slit width ($300 \mu m$) corresponded to $1.8''$ and the length of each slit segment, in front of each array, to $6''$. Wavelength coverage was $3500 - 7000 \mathring{A}$, with peak sensitivity in the blue.

Normal reduction procedures have been carried out, using software written by D. O'Donoghue and J. Menzies, on the University of Cape Town Vax 6230 computer. Cal-

ibration arcs were fitted with 5^{th} order polynomials. Various templates for the cross-correlation measurement of absorption line redshifts were examined. The best proved to be a template made from a mixture of several G and K-type radial-velocity standard stars. Various checks (*e.g.*, manual versus cross-correlation, reduction of calibration arc as if it were a galaxy) have been carried out to ensure that there were no hidden errors in the software.

Due to the faint magnitudes of the target galaxies, we opted for a low dispersion in the spectrograph: the pixel width (near maximum instrumental sensitivity) corresponds to about $200\,km\ sec^{-1}$ in radial velocity. True external errors - standard deviations and systematic shifts - can be established using the observations of the radial-velocity standard stars. When the cross-correlation template was run against the eight individual stars that comprise it, a standard deviation of only $18\,km\ sec^{-1}$ was found. However, a more realistic measure results when the radial velocity standards, observed in the three observing periods, were run against each other. In this way a standard deviation of $35\,km\ sec^{-1}$ was determined, with cross-correlation contrast factors of $r > 10$. This value can be taken as the minimum external error for the system, as used in this observing program.

If the galaxies were bright and their peak counts per channel comparable to those of the the radial velocity stars (> 500), the errors would be of this order. Obviously, this is not the case. The errors listed in the accompanying table are derived from r contrast factors, with the constraint that the error tends down to $35\,km\ sec^{-1}$ as $r > 10$ and rises to $250\,km\ sec^{-1}$ for a marginal contrast of $r = 2.0$. The $250\,km\ sec^{-1}$ is established from comparing velocities, previously derived with the same instrumentation, to those from other investigators (see below). No significant systematic errors were found, but a small offset ($28\,km\ sec^{-1}$) was applied to the 1992 run as indicated by the standard radial-velocity stars. The cross-correlation is not used blind; manual checks are made for each galaxy. For faint marginal galaxies, the cross-correlation is sometimes replaced by manual measurements, with appropriate estimated errors. The aim is always to provide a true external error. One of us (AF) has found that true external errors are typically twice the errors claimed by other authors. This became quite obvious while cataloguing galaxy redshifts (Fairall and Jones, 1991) and comparing multiple radial-velocity measurements and their quoted errors for a given galaxy.

In the case of emission lines, an error of $100\,km\ sec^{-1}$ has been assumed for a single line. Thus the error is $70\,km\ sec^{-1}$ when two lines are used for determining an average, $58\,km\ sec^{-1}$ when three lines are used, etc.

2.2. Results

In this way we have observed 142 objects in the three weeks of observing time allocated to this program in 1991 and 1992. The results based on the observations at the SAAO are presented as follows: we first concentrate on the galaxies for which a good S/N redshift could be deduced (2.2.1). This is then compared to other redshift determinations in 2.2.2. The modest 1.9m aperture of the telescope meant that only the brighter end of the apparent luminosity distribution could be observed. Even so, about 20% of the observed galaxies proved too faint to extract a reliable redshift from the spectrum. They and other galaxies for which no reliable redshift could be obtained are described in 2.2.3. As discussed before, we aimed at getting redshifts for all the brighter galaxies in our search area. The largest of the galaxies in the ZOA ($D \gtrsim 1 arcmin$) were known before our deep galaxy survey and some of them have already been observed. As these galaxies are relevant to our investigation they are listed 2.2.4. In the next section (2.2.5) we then turn to a discussion of the typical properties of the galaxies observed in the ZOA.

2.2.1. Galaxies with redshifts from the SAAO observations

In Table 1, the 116 galaxies for which a reliable velocity could be deduced are listed. The positions and the most relevant properties, such as large and small diameters, magnitudes and morphological types, are taken from KK94 and a detailed discussion of these parameters is given in the catalogue there. It must be emphasized again that the observed properties such as diameters and magnitudes are severely reduced by the dust screen of the Milky Way. Even at the highest latitudes ($|b| \approx 8 - 10°$) the galaxies suffer a foreground extinction of about 1 mag, decreasing *e.g.*, the visible diameter to $\approx 75\%$. The extinction increases dramatically as we approach the galactic dust equator. The galaxies in the deepest extinction layer – which are still barely visible – are seen through an obscuration layer of $A_B \approx 5\overset{m}{.}0 - 6\overset{m}{.}0$. Their true diameters will be a factor $\approx$ 8-10 larger than seen on the IIIaJ plates. The properties listed in Table 1 are the *observed* properties uncorrected for extinction (and always are underestimates).

The entries in Table 1 are as follows:

Column 1 and 2: Identification of galaxy as given in KK94 and Lauberts Identification (Lauberts, 1982).

Column 3 and 4: Right Ascension and Declination (1950.0). The positions were measured with the measuring machine Optronics at the ESO in Garching and have an accuracy of about 1 arcsec.

Column 5 and 6: Galactic longitude ℓ and latitude b.

Column 7: Large and small diameter (in arcsec). The diameters are measured approximately to the isophote of 24.5 mag arcsec^{-2} and have a scatter of $\sigma \approx 4''$.

Column 8: Apparent magnitude B_J. The magnitudes are estimates from the IIIaJ film copies of the ESO/SRC Survey based on the above given diameters and an estimate of the average surface brightness of the galaxy. A preliminary analysis of this data finds a linear relation

Table 1. Galaxies with radial velocities obtained at the SAAO

Iden.	Laub. Iden.	RA (1950.0)	Dec (1950.0)	gal. long.	gal. lat.	D x d arcsec	B(J)	Type	v(hel) er abs		v(hel) er em		Identified Em. lines	Rm
1	2	3	4	5	6	7	8	9	10	11	12	13	14	15
58		8 33 35.2	-56 27 7	272.79	-9.63	22x 20	16.8	S 3	13857	200	14111	58	1 3 6	
59	L165- 1	8 33 36.1	-57 28 22	273.63	-10.23	141x 34	14.8	S 2	4178	92				
67		8 33 46.0	-55 0 22	271.62	-8.76	50x 34	15.7	S 0			4299	50	1 3 6 7	
87		8 34 19.6	-54 32 39	271.29	-8.42	47x 23	16.2	F	9386	178	8853	70	5 6 7	
165		8 36 8.0	-55 24 47	272.16	-8.73	31x 24	16.6	F	18426	83				
170		8 36 14.2	-56 36 51	273.14	-9.43	24x 17	17.0	F	21101	82				
197		8 36 45.7	-57 47 49	274.15	-10.08	34x 17	16.9	E	18159	124				
213		8 37 3.4	-55 0 4	271.90	-8.38	38x 24	16.4	F	12432	78				
368		8 42 1.4	-53 30 51	271.16	-6.90	70x 20	16.0	S E	7831	104				
373		8 42 9.3	-56 1 34	273.17	-8.43	67x 47	15.0	E 2	2754	68				
401		8 43 25.9	-56 53 39	273.97	-8.82	34x 27	16.2	L	18408	83				
421		8 44 7.2	-56 54 41	274.04	-8.76	40x 34	16.1	S	17886	228				
445		8 44 52.7	-54 57 2	272.55	-7.46	36x 36	16.1	E 0	12736	87				
459		8 45 16.2	-58 55 20	275.74	-9.87	34x 23	16.5	S 0	16544	237				
527		8 47 53.8	-55 34 54	273.32	-7.52	23x 20	16.7	E ?			19692	70	2 3 4 5	1
656		8 52 10.9	-58 56 16	276.32	-9.19	54x 20	16.2	L	6951	168				
661		8 52 24.3	-60 14 12	277.36	-9.99	54x 15	16.5	S M	20214	118				
694	L165- 7	8 53 32.8	-55 41 58	273.93	-6.98	67x 13	16.3	S ?	10110	100	10049	100	6	
698		8 53 43.5	-58 43 36	276.29	-8.90	67x 50	15.2	E	2483	148				
787		8 57 4.8	-59 41 43	277.32	-9.19	54x 30	15.6	S M	24016	300				
889		9 0 56.2	-58 42 54	276.89	-8.18	62x 28	15.9	S 1	10361	73				
936		9 2 27.0	-56 5 49	275.05	-6.29	24x 16	17.1	F	10278	194				
986		9 4 25.2	-55 10 51	274.55	-5.47	40x 9	17.1	S 1	9832	167				
1083	L125- 9	9 9 4.5	-58 21 35	277.34	-7.15	70x 35	15.4	S R5	2928	400	2815	100	6	
1104		9 9 57.9	-55 40 15	275.45	-5.23	16x 16	17.3	E 0:	9877	88				
1229		9 18 6.8	-59 21 39	278.89	-7.00	27x 19	16.4	E 2	10311	95				
1250		9 20 17.4	-59 13 10	278.98	-6.71	60x 13	16.1	S 2	9886	185				
1259		9 20 51.4	-59 15 35	279.06	-6.68	27x 17	16.4	S 0	10447	82				
1272		9 21 28.3	-56 55 44	277.47	-4.97	24x 15	17.1	S L	7350	500	6724	70	6 7	
1288	L 91- 11	9 22 18.2	-63 27 50	282.18	-9.54	101x 12	15.8	S 3			3192	70	5 6 7	
1345	L126- 12	9 25 53.2	-62 20 59	281.69	-8.46	54x 20	16.2	S E	10288	175				
1371	L126- 14	9 27 6.5	-60 34 56	280.56	-7.08	87x 47	14.4	E 5	2273	132				
1382		9 27 54.8	-59 46 56	280.08	-6.44	17x 13	17.4	E 3	10266	124				
1397	L126- 17	9 28 42.0	-61 57 44	281.66	-7.95	108x 60	13.9	S 0	2844	93				
1484	L126- 21	9 35 10.9	-61 52 25	282.16	-7.37	51x 47	14.8	L	4585	101				
1517	L126- 24	9 37 8.0	-61 36 9	282.15	-7.01	108x 74	13.8	S 4	2847	135				A
1519	L126- 25	9 37 12.5	-61 30 38	282.10	-6.94	54x 40	14.9	L	2792	64				
1522	L 91- 17	9 37 17.1	-63 42 27	283.58	-8.57	87x 60	14.6	S 2	4657	104				
1547		9 39 25.8	-48 46 9	273.94	2.87	20x 20	17.0	S E	17476	162				
1561		9 40 18.1	-60 34 10	281.75	-5.98	34x 20	16.2	E 4	3268	300	3070	70	3 6 7	
1577		9 41 15.8	-63 47 32	283.97	-8.35	31x 27	16.3	S 0	18458	300				
1600		9 42 57.5	-64 43 57	284.73	-8.94	22x 16	17.2	L	16272	150				
1624		9 44 46.1	-47 53 55	274.05	4.11	17x 17	17.1	E ?	17023	157				
1664	L213- 2	9 47 22.9	-47 41 9	274.26	4.55	101x 94	13.2	L	1890	50				
1685	L213- 3	9 48 43.1	-49 28 40	275.56	3.30	54x 40	15.3	S 5:	12391	500				
1735		9 51 33.2	-50 47 33	276.74	2.56	16x 16	17.3	E 0	11565	115				
1758		9 53 16.8	-49 11 57	275.97	3.98	24x 13	17.0	S 2			7745	58	3 6 7	
1786		9 54 25.2	-49 59 41	276.61	3.47	34x 32	15.4	E	6932	115				
1808	L 92- 1	9 55 29.1	-65 23 17	286.18	-8.61	74x 54	14.6	E 3	5571	150				
1853		9 58 4.7	-64 29 26	285.85	-7.73	47x 34	15.4	E			1728	41	1 3 4 5 6 7	B
1856	L 92- 3	9 58 14.7	-67 3 53	287.45	-9.76	101x 34	14.9	S 1	1478	207				
1875		9 59 24.3	-63 49 11	285.55	-7.11	51x 22	15.9	S 1:	10048	142				
1920		10 2 55.2	-66 34 7	287.52	-9.09	56x 56	15.0	L	2081	84				
1939	L213- 6	10 4 11.8	-50 21 59	278.09	4.11	54x 16	16.1	I			5262	80	6	
1949	L263- 4	10 4 47.4	-47 27 5	276.45	6.53	74x 47	14.6	SB 3	3971	212	4002	100	6 7	
1963	L 92- 10	10 5 32.4	-64 7 6	286.28	-6.95	74x 74	14.3	S 3			57	58	1 3 4 5 6 7	2
2006		10 7 43.6	-48 44 31	277.60	5.76	47x 13	16.8	S 3:	11769	121				
2033		10 9 8.6	-48 52 51	277.88	5.79	20x 17	17.2	L	5696	124				
2040	L 92- 14	10 9 29.4	-66 24 2	287.96	-8.57	87x 51	14.2	F	1876	35				
2081		10 11 8.4	-63 46 59	286.59	-6.32	34x 11	16.9	S 0			3258	50	1 3 6 7	
2103	L213- 8	10 11 44.8	-49 48 17	278.76	5.27	34x 27	15.9	SB 3	6741	200	6774	100	6	
2105		10 11 49.6	-49 24 36	278.54	5.60	20x 20	17.1	E ?	5818	88				
2109	L213- 9	10 11 50.9	-52 2 16	280.03	3.43	47x 40	15.3	SB 3			2709	70	3 6	
2114		10 12 4.7	-51 30 41	279.76	3.89	34x 9	17.1	S 3:			2948	50	1 3 5 6	
2140	L 92- 17	10 12 48.4	-64 39 25	287.24	-6.94	74x 40	15.3	S 1	3882	180				
2182		10 14 22.0	-67 40 28	289.08	-9.34	40x 15	16.5	S 1	2027	100	2016	100	6	
2196		10 14 49.2	-50 56 2	279.80	4.61	34x 27	16.0	F	14167	200				
2197		10 14 50.1	-48 49 46	278.62	6.36	34x 20	16.3	SB 4	16408	300				
2209		10 15 7.0	-50 9 44	279.41	5.27	20x 13	17.2	L	8537	171				
2250		10 16 25.0	-51 40 4	280.41	4.13	50x 12	16.9	S ?	19180	400	18892	100	1	

Table 1. – continued

Iden.	Laub. Iden.	RA (1950.0)	Dec	gal. long.	gal. lat.	D x d arcsec	B(J)	Type	v(hel) abs	er	v(hel) em	er	Identified Em. lines	Rm
1	2	3	4	5	6	7	8	9	10	11	12	13	14	15
2280		10 17 2.7	-47 51 57	278.40	7.36	44x 40	15.5	S 1	13828	192				
2284		10 17 11.4	-49 26 1	279.28	6.07	54x 44	15.4		19144	138				
2313		10 17 45.7	-49 47 39	279.56	5.82	47x 23	16.1	S E:	5741	300				
2326		10 18 9.5	-48 26 41	278.87	6.98	34x 7	17.5	S 1	15147	148				
2341		10 18 35.5	-63 45 52	287.27	-5.85	47x 31	15.7	L			3783	45	1 4 5 6 7	
2360		10 19 11.0	-48 30 8	279.05	7.02	31x 19	16.6	S M	5296	300				
2363		10 19 17.7	-48 46 26	279.21	6.81	38x 19	16.6	L	6571	300				
2378 L 92- 21		10 19 36.2	-66 14 22	288.71	-7.86	74x 60	14.5	L	2002	52				
2434		10 21 20.8	-53 35 44	282.09	2.92	20x 13	17.0	E 3	9586	300				
2469 L168- 2		10 22 49.9	-54 32 40	282.78	2.23	101x 13	15.7	S 4			996	70	5 6	
2487		10 23 27.6	-51 43 8	281.36	4.68	13x 8	18.6	E	12029	183				
2490		10 23 29.0	-51 42 47	281.36	4.68	27x 9	17.7	S E	12097	141				
2491		10 23 30.6	-49 36 24	280.25	6.47	27x 20	16.9	F	14554	133				
2508 L 62- 10		10 24 4.9	-67 29 26	289.77	-8.68	60x 60	14.9	SX 7	6023	100	6011	70	3 6 7	3
2544 L214- 6		10 25 14.4	-48 52 20	280.10	7.25	67x 16	16.1	S 2	5978	173				
2546		10 25 16.6	-48 51 37	280.10	7.26	51x 43	15.3	S 1	5492	132				
2579 L214- 7		10 26 13.9	-50 15 36	280.97	6.15	54x 32	15.7	SB	5620	250				
2584		10 26 19.7	-51 40 57	281.72	4.94	32x 15	16.7		9873	400				
2591		10 26 31.8	-50 8 8	280.94	6.28	27x 20	16.8	E 3	7041	98				
2595 L214- 10		10 26 42.5	-50 42 53	281.27	5.80	81x 22	15.6	S 1	6362	220				
2598 L214- 11		10 26 46.2	-50 26 35	281.14	6.04	67x 32	15.4	S 1	6305	142				
2608		10 27 27.1	-67 15 28	289.92	-8.31	40x 13	16.6	S 0	5895	188	6039	100	6 7	
2614		10 27 43.2	-49 19 54	280.69	7.07	44x 27	16.0	L	14016	168				
2620 L214- 12		10 27 54.8	-49 59 9	281.06	6.52	60x 35	15.6	S ?	15879	142				
2646		10 28 48.7	-49 48 45	281.09	6.75	54x 23	16.2	S 4	12442	200				
2659		10 29 22.1	-51 7 14	281.84	5.67	40x 19	16.3	E			6537	70	1 6	
2672		10 29 57.1	-49 48 15	281.25	6.85	27x 13	17.3	S E	19330	184				
2684 L 92- 22		10 30 14.5	-63 27 2	288.21	-4.90	128x 47	14.6	S 7	3671	210				
2733		10 33 22.1	-67 27 48	290.52	-8.20	40x 35	15.7	S 1			5953	70	3 6	
2768		10 36 19.2	-52 45 39	283.59	4.78	34x 12	16.3	S E	15411	200				
2847 L169- 2		10 46 9.0	-53 2 18	285.04	5.23	94x 27	15.2	S L			2712	80	6	
2877		11 0 3.3	-52 41 48	286.79	6.45	27x 16	16.8	E 3	3947	143				
2879 L169- 5		11 0 20.4	-53 22 26	287.11	5.85	67x 47	14.9	SB 1	3766	146				
2919		11 17 1.5	-54 40 30	289.88	5.57	27x 11	17.1	S E:	12172	143				
2921		11 17 7.8	-53 27 39	289.47	6.71	27x 13	17.0	S M?	7417	200				
2985		11 23 6.5	-53 1 14	290.17	7.43	40x 12	16.8	S E	14975	300				
2992 L170- 3		11 23 48.9	-53 57 37	290.58	6.58	94x 40	14.6	S 2	5369	167				C
2995 L170- 4		11 24 21.2	-53 58 51	290.66	6.58	112x 17	15.8	S M	5742	200				
3017		11 26 41.1	-58 8 49	292.30	2.74	74x 34	15.3	SX 3	4639	207				
3024		11 27 33.8	-55 11 37	291.49	5.58	38x 35	15.8	E 0	4260	157				
3051		11 29 50.9	-53 20 49	291.24	7.44	27x 20	16.9	E	16945	84				
3157		11 36 13.6	-54 33 32	292.50	6.55	40x 31	16.2	S M	12322	143				
3229		11 43 56.6	-54 45 33	293.64	6.66	24x 13	17.3	L	14043	102				
3238		11 44 44.1	-52 24 16	293.16	8.97	20x 16	17.3	E 2	15479	229				
3257		11 47 7.3	-52 35 19	293.56	8.88	47x 19	16.1	E 6			4502	70	3 6	
3279		11 50 6.7	-57 0 33	295.02	4.68	81x 54	14.7	S E	5355	167				

from the brightest to the faintest galaxies ($B_J \approx 19^m.5$) with a scatter of only $\sigma \approx 0^m.5$.

Column 9: Morphological type. The morphological types are coded similarly to the precepts of the RC2 (de Vaucouleurs *et al.* 1976). Due to the varying foreground extinction a homogenous and detailed type classification could not always be accomplished and some codes were added. In the first column F for E/S0 was added to the normal designations of E, L, S and I. In the fourth column the subtypes E, M and L are introduced next to the general subtypes 0 to 9. They stand for early spiral (S0/a-Sab), middle spiral (Sb-Sd) and late spiral or irregular (Sdm-Im). The cruder subtypes are a direct indication of the fewer details visible in the obscured galaxy image. The questionmark at the end marks uncertainty of the main type, the colon uncertainty in the subtype.

Column 10 and 11: Heliocentric velocity and error as derived from the absorption features ($km\ sec^{-1}$). The errors may appear large as they are estimated external errors, and not internal errors (see Sect. 2.1).

Column 12 and 13: Heliocentric velocity and error measured from the emission lines (identified in column 14) when present ($km\ sec^{-1}$).

Column 14: Identified emission lines. The codes 1-7 are explained in the table below, where the 1^{st} line gives the code of the emission lines used for the redshift evaluation, the 2^{nd} line names the emission lines, and the

3^{rd} line lists the corresponding wavelengths in $\AA$:

1	2	3	4	5	6	7
[OII]	Hγ	Hβ	[OIII]	[OIII]	Hα	[NII]
3727	4340	4861	4959	5007	6563	6584

Column 15: Code for additional remarks:

1 – The spectrum of KK527 shows this to be a Seyfert 1 galaxy.

2 – The spectrum of KK1963=L92-10 was measured at different sites and – based on the emission lines [OII], Hβ, [OIII], Hα, [NII] – the following velocities were obtained: $v_{hel} = 134, 26, 87, 10, 35, 6, 100 \pm 58\, km\ sec^{-1}$. The velocity given in Table 1 is the mean of all these velocities. Further details are given below.

3 – Due to superposition of a star on the galaxy KK2508=L62-10 the exposures were centred slightly west of the centre of the object.

For some of the galaxies other redshift measurements are availabale as well (cf. section 2.2.2):

A – $v_{hel} = 2916 \pm 45\, km\ sec^{-1}$ by Strauss *et al.* 1992, for KK1517=L126-24.

B – $v_{hel} = 1830\, km\ sec^{-1}$ by Acker *et al.* 1991 for KK1853 (cf. special cases).

C – $v_{hel} = 5523\, km\ sec^{-1}$ by Dressler 1991 for KK2992=L170-3.

Special cases:

L166–P18 A very intriguing galaxy candidate was detected in the galaxy search at $9^h29^m08\overset{s}{.}8 - 52°56'43''$. It lies extremely close to the actual dust equator ($\ell = 275\overset{\circ}{.}5$, $b = -1\overset{\circ}{.}3$) and was one of the primary candidates for a highly obscured nearby large galaxy. It has a very high surface brightness, is clearly elongated (23″ x 15″) with small protrusions at the end of the major axis which turn off at opposite angles from the main body. It looks like the most inner part of a early type (barred?) spiral galaxy. However, the spectrum we obtained at the SAAO clearly proved this to be a planetary nebulae – as categorised in Lauberts (1982) – with its emission lines Hβ, [OIII], Hα and [NII], and line ratios typical for PN's. The mean velocity of this object is $v_{hel} = 7 \pm 58\, km\ sec^{-1}$.

In the course of our galaxy search, further PN-candidates have been found. We have observed these as well and so far discovered 2 new planetary nebulae. This is reported in Kraan-Korteweg *et al.* 1994b.

KK1853=L92–G?02 This fairly bright elliptical galaxy at ($\ell = 285\overset{\circ}{.}9$, $b = -7\overset{\circ}{.}7$) has been misidentified in earlier years as a planetary nebula. In 1991, Acker *et al.* started a project to get spectra of all misidentified PN. During this effort, KK1853 was confirmed to be an emission line galaxy – as found here.

KK1963 = L92–G10 The morphology of this object suggests this to be a nearby spiral galaxy. It has a patchy appearance, is quite extended (74″ x 74″) and the estimated magnitude is about $B_J = 14\overset{m}{.}3$. It lies at $\ell = 286\overset{\circ}{.}3$, $b = -6\overset{\circ}{.}9$ in the Milky Way, hence is seen through a non-negligible extinction layer. Its true dimensions will be considerably larger and it could well be a fairly local galaxy. However, its identification as a galaxy is still questionnable. In Lauberts (1982) it was classified as an emission nebula *or* galaxy, and in the Southern Galaxy Catalogue (Corwin *et al.* 1985) as an irregular galaxy of type IB(s)m?. The object has an entry in the IRAS Point Source Catalog. The fluxes in Jy at the 4 wavebands are $f_{12} = 0.42L$, $f_{25} = 0.25L$, $f_{60} = 2.94$ and $f_{100} = 5.74$; L indicates that it is a lower limit only. The colors are compatible with it being a galaxy (*e.g.*, Meurs and Harmon, 1988, Lu *et al.* 1990). But since the signature of various galactic objects are similar to galaxies as a whole, this is not really decisive.

We did various exposures at different positions on this object and found strong emission all over. The systemic velocity – taken as the mean of the emission features at the different locations – is of $v = 57\, km\ sec^{-1}$. The correction of this observed velocity to the centroid of the Local Group is quite large ($\Delta = -299\, km\ sec^{-1}$, in accordance to the precepts given in the RSA, cf. Sandage and Tammann 1981) and the corrected recession velocity is $v_0 = -242\, km\ sec^{-1}$. Based on this velocity, the regarded object is more likely to be a galactic object than a new member of the Local Group as its velocity is more negative than any of the other known members of the Local Group.

KK2463 = L168-G02 This galaxy is the only one in the search area with a velocity less than $1000\, km\ sec^{-1}$, namely $v = 996\, km\ sec^{-1}$, respectively $v_0 = 689\, km\ sec^{-1}$ when corrected to the centroid of the LG. It does not lie in any known group. The nearest known group is the CenA group at $l \approx 310°, b \approx 20°$ and $v_0 \approx 275\, km\ sec^{-1}$ which definitely is too far apart on the sky as well as in velocity space to be related.

The galaxy is an extended very LSB spiral (Sbc) at very low latitude ($\ell = 282\overset{\circ}{.}8$, $b = 2\overset{\circ}{.}2$). Based on the HI-column density (Kerr *et al.* 1986) and the relation between HI and extinction as given in Burstein and Heiles (1982) the extinction is estimated to be at least of the order of $A_B \approx 2\overset{m}{.}5$. Considering that the observed properties are 101″ x 13″ and $B_J = 15\overset{m}{.}7$, the extinction-corrected diameters will roughly be about a factor of 3 larger, making it an edge-on spiral of about 5 arcmin with an absorption-corrected magnitude of $B_J^0 \approx 12\overset{m}{.}5$ (cf. Cameron 1990). There seem to be a number of similar, extended LSB objects in the vicinity of this galaxy at even lower latitudes. It is therefore not unlikely that this galaxy is part of a nearby, previously unrecognized group which then would not be unimportant with regard to the dynamics in the local neighbourhood.

2.2.2. Comparison of the SAAO-redshifts to other values

We concentrated mainly on observing galaxies without previously measured velocities. A comparison of our redshifts with other (published) determinations is only possible for 3 of the galaxies in Table 1, *i.e.*, KK1517, KK1853, KK2992. The velocity values and their sources are given in the remarks to Table 1. A comparison between our velocities and the measurements from the literature finds:

$$< v_{SAAO} - v_{pub} >= -106 \pm 26\, km\ sec^{-1}\,.$$

With the exception of KK1853, the differences are well within the errors quoted in Table 1. The offset of $-106\, km\ sec^{-1}$ is quite large. It is, however, only based on 3 independent sources, each for a different galaxy, and therefore not really significant. This is confirmed by our complementary observing programs: 10 of the galaxies observed at the SAAO are in dense regions and were also observed with the multifiber system Optopus. The offset between these observations is

$$< v_{SAAO} - v_{OPT} >= +19 \pm 75\, km\ sec^{-1}\,,$$

hence negligible. The individual differences are within the quoted errors. In addition, 7 of the galaxies observed here have meanwhile been observed by us at Parkes in HI. The agreement is excellent and the mean difference is only

$$< v_{SAAO} - v_{PKS} >= +31 \pm 20\, km\ sec^{-1}\,,$$

with a very small dispersion.

Overall the correspondence between the radial velocities measured at the 1.9m telescope of the SAAO and the redshifts derived from other observing programs is very good and well within the quoted errors.

2.2.3. Galaxies without reliable redshifts

For 25 of the observed galaxies no reliable redshift could be determined. For three galaxies the bulk of the spectrum was due to a superimposed foreground star. For three other galaxies a tentative identifaction based solely on the Mg absorption line at $5175\mathring{A}$ could be made, but as no other features in accordance with the indicated redshift could be found, the deduced values are too uncertain. No reliable feature could be indentified in 7 of the observed galaxies. For 12 further galaxies the S/N was too low. Some of these galaxies are just too faint for detection with the 1.9m telescope even though their apparent brightness is quite bright (cf. column 8 in Table 2), but they are extended very low surface-brightness spirals. Such galaxies are likely to be nearby spirals. We have observed these in Parkes (Kraan-Korteweg, Henning, Schröder and van Woerden, in preparation) and the majority of them have been detected and confirmed to be nearby ($v < 5500\, km\ sec^{-1}$).

The galaxies for which no reliable redshift could be extracted are listed in Table 2. Columns 1 to 9 are the same as for Table 1 and lists names, positions and properties of the galaxies (cf. explanations to Table 1 for further details). The remark in column 10 describes the reason for the non-detection.

2.2.4. Galaxies with redshifts from the literature

The redshifts of 31 galaxies in the ZOA in the Hydra/Antlia search area have been determined by others. This concerns mainly bright and large galaxies ($D > 1 arcmin$), plus some IRAS-galaxies within $5° < |b| < 10°$ identified by Strauss *et al.* 1992 for their 2Jy IRAS Redshift Survey. On average, these are galaxies which would have entered our observing list, if there redshift had not been measured by others. They are relevant for the discussion of the observed sample as a whole and these galaxies are listed in Table 3.

Columns 1-9 are the same as in Table 1, and details about the entries can be found there. Column 10 and 11 list the heliocentric velocities and errors (if given). The velocity in column 10 has been adopted from the source identified in column 12, where (1) stands for *The Southern Redshift Catalogue and Plots* by Fairall and Jones (1991), and (2) for *The General Catalog of HI-Observations of Galaxies* by Huchtmeier and Richter (1989). The original sources can be looked up there. (3) are velocities measured by Strauss *et al.* (1992) for the 2Jy IRAS Redshift Survey.

2.3. Description of Observed Sample

In Fig. 2 we have plotted in galactic coordinates the distribution of all the galaxies in the Hydra/Antlia search region for which a radial velocity is now available, *i.e.*, the 115 galaxies for which we determined a redshift at the SAAO (filled dots) as well as the 31 galaxies with redshifts from the literature (open dots), hence 146 galaxies in total. The 25 observed galaxies for which no redshift could be determined are not displayed, nor the uncertain galaxy with $v_0 = -242\, km\ sec^{-1}$ and the observed PN.

As discussed in the introduction, we aimed primarily at obtaining radial velocities for all the brightest galaxies in the Hydra/Antlia search, or more accurately due to the restrictions of the 1.9m telescope for all galaxies with high central surface brightness. At the same time, a representative coverage of the overall galaxy distribution was attempted. Our selection criteria were softened towards the galactic equator where a larger fraction of relatively faint and small galaxies entered our observing program, as we tried to trace the galaxy distribution as deep as possible into the dust equator where the extinction is highest and the diminishing effects largest. This is partly reflected in the distribution here. Overall, the achieved distribution of galaxies with radial velocities seems a fair tracer of the galaxy distribution in the ZOA – compared to the distri-

Table 2. Galaxies observed at the SAAO without reliable redshift

Iden.	Laub. Iden.	RA (1950.0)	Dec	gal. long.	gal. lat.	D x d arcsec	B(J)	Type	Remark
1	2	3	4	5	6	7	8	9	10
124		8 35 9.7	-57 9 3	273.49	-9.87	38x 31	16.0	E	s.p.* spec.
300		8 39 44.1	-54 41 10	271.88	-7.88	54x 13	16.5	S E	No rel.feat.
686		8 53 13.4	-55 36 33	273.83	-6.95	58x 40	15.4	S L	S/N too low
1129	L 91- 2	9 11 27.8	-62 59 50	280.98	-10.10	60x 20	15.9	S 3	No rel. feat.
1551		9 39 36.1	-65 4 33	284.69	-9.43	40x 19	16.6	S 1	S/N too low
1595		9 42 41.3	-62 22 51	283.16	-7.17	34x 9	17.2	S 1?	S/N too low
1637		9 45 19.7	-60 20 21	282.08	-5.41	22x 17	17.1	S M	No rel.feat.
1767		9 53 47.	-61 42.9 :	283.75	-5.83	27x 20	16.5	S 4	No rel.feat.
1854		9 58 5.9	-49 29 16	276.77	4.23	27x 13	17.0	S M	Mg 5175 only
1862	L 92- 4	9 58 32.6	-67 24 7	287.68	-10.01	114x 47	14.6	S 1	S/N too low
1945		10 4 34.2	-49 59 53	277.92	4.44	47x 40	15.1	SBR4	Mg 5175 only
2032		10 9 7.4	-48 53 26	277.88	5.78	34x 13	16.9	S ?	s.p.* spec.
2108		10 11 50.8	-48 41 1	278.13	6.20	40x 16	16.0	SX	No rel.feat.
2142		10 12 52.4	-47 28 55	277.59	7.29	40x 20	16.3	SB 4	S/N too low
2359		10 19 5.7	-47 24 36	278.43	7.93	32x 22	16.5	S M	S/N too low
2445		10 21 47.4	-47 57 12	279.12	7.72	34x 34	16.2	S R2	No rel.feat.
2522	L214- 5	10 24 44.0	-48 54 27	280.04	7.17	22x 19	17.0	E 0	s.p.* spec.
2585	L214- 8	10 26 23.3	-50 26 7	281.08	6.01	65x 47	14.9	S M	S/N too low
2639		10 28 33.7	-49 40 20	280.98	6.85	27x 9	17.4	E 7	S/N too low
2855		10 46 49.4	-51 41 38	284.52	6.48	27x 15	17.0	L ?	S/N too low
2909		11 13 2.0	-53 39 33	288.97	6.31	23x 11	17.2	SB 1	Mg 5175 only
3003		11 24 50.2	-57 56 4	292.00	2.86	22x 16	17.0		S/N too low
3154	L170- 8	11 36 0.8	-52 47 3	291.97	8.25	47x 16	16.6	L	S/N too low
3191		11 39 24.8	-52 33 51	292.41	8.60	17x 16	17.3	E 2	No rel.feat.
3245	L170- 12	11 45 29.4	-53 37 32	293.57	7.81	47x 34	16.0	S 5	S/N too low

Table 3. Galaxies with radial velocities from the literature

Iden.	Laub. Iden.	RA (1950.0)	Dec	gal. long.	gal. lat.	D x d arcsec	B(J)	Type	v(hel)	er	S
1	2	3	4	5	6	7	8	9	10	11	12
162	L165- 2	8 36 5.0	-54 56 51	271.77	-8.46	242x215	12.0	L	1051	39	3
659		8 52 17.6	-59 1 35	276.40	-9.23	91x 89	14.0	E 1	2715		1
799		8 57 31.4	-55 12 26	273.92	-6.23	24x 19	17.0		25150	36	3
943		9 2 47.4	-57 57 38	276.48	-7.50	17x 9	18.3	S M	16439	14	3
1125	L126- 1	9 11 17.4	-58 38 6	277.74	-7.13	56x 34	15.2	S 3:	2874	50	1
1146	L126- 2	9 12 16.1	-60 34 56	279.26	-8.38	67x 60	14.3	SB 2	2900		1
1159	L126- 3	9 13 23.0	-60 13 30	279.09	-8.03	114x 67	13.6	SB 4	2857	35	1
1161	L126- 4	9 13 28.6	-60 32 12	279.33	-8.24	67x 60	15.2	SBS5	3287		2
1170	L 91- 4	9 14 29.1	-62 51 37	281.12	-9.75	121x 94	13.5	S 1	2970		1
1196	L 91- 7	9 16 21.9	-62 40 19	281.13	-9.47	121x 81	13.4	S 5	2411		2
1265	L126- 10	9 21 8.3	-60 50 5	280.21	-7.77	121x 40	14.1	S 3	2107	38	3
1286	L 91- 9	9 22 16.2	-63 35 49	282.27	-9.64	134x 94	13.6	E	2870		1
1353	L126- 13	9 26 12.6	-60 33 07	280.46	-7.14	128x 47	14.3	S 1	2503		2
1506	L126- 23	9 36 31.6	-61 55 31	282.31	-7.30	114x 47	14.2	S 3	2759	43	3
1514	L 91- 16	9 36 57.6	-63 15 38	283.25	-8.26	108x 27	14.9	S 0	2069	35	3
1524		9 37 19.5	-63 44 46	283.61	-8.60	54x 40	15.4	SB 1	4523	36	3
1628	L 91- 18	9 44 48.0	-63 2 24	283.78	-7.52	141x 16	15.1	S 2	3195	20	2
1907	L 92- 6	10 1 54.6	-64 43 26	286.32	-7.67	148x 87	13.5	SXR3	2437	20	2
1943	L 92- 8	10 4 30.8	-67 8 2	287.99	-9.45	215x161	12.3	E 3	1691		1
2000	L 92- 12	10 7 30.2	-66 47 2	288.02	-8.99	195x 74	13.1	SB 3:	1367		1
2026	L 92- 13	10 8 51.9	-66 45 30	288.11	-8.89	98x 81	13.8	E 4	1786		1
2063	L127- 11	10 10 36.5	-62 17 11	285.69	-5.12	67x 27	15.1	S 3	3370	36	3
2200	L213- 11	10 14 55.2	-48 37 47	278.52	6.53	269x175	12.0	SB 4	2741	8	1
2759		10 35 33.8	-52 18 37	283.27	5.12	28x 11	17.1	S	6320	37	3
2852		10 46 22.0	-65 3 34	290.53	-5.47	27x 27	16.6		3360	41	3
2870	L 93- 3	10 57 32.6	-66 3 51	292.01	-5.87	94x 47	14.7	S 3	1470	150	1
2902		11 11 12.6	-67 15 45	293.74	-6.43	60x 34	15.7	SB 5	5762	37	3
2991	L170- 2	11 23 43.3	-52 30 16	290.09	7.95	81x 81	14.5	SBR5	4941		1
3176	L170- 10	11 37 39.5	-54 7 13	292.58	7.03	60x 54	15.1	SB 4	4676		1
3204	L216- 35	11 41 37.1	-52 20 0	292.67	8.91	74x 67	14.9	S S5	4446		1
3228	L170- 11	11 43 39.4	-56 6 37	293.94	5.34	202x108	12.8	S 4?	1901	36	3

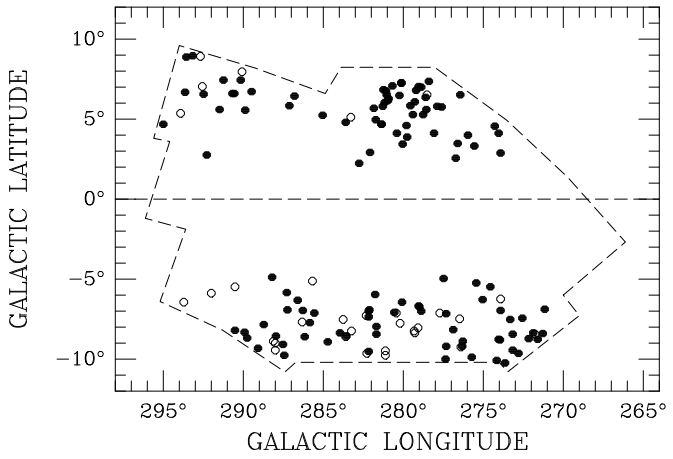

Fig. 2. Distribution of the galaxies with radial velocities. The Hydra/Antlia survey region is outlined. Filled dots are objects observed by us at the SAAO; open dots are galaxies with redshifts from other sources.

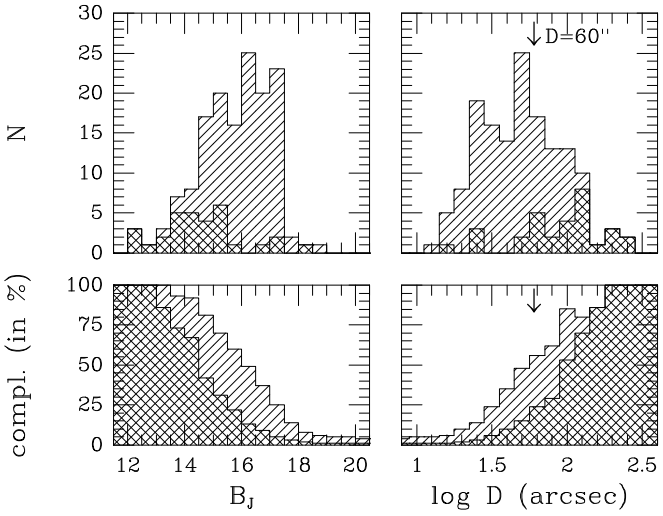

Fig. 3. Magnitude and major-axis diameter distribution of galaxies with radial velocities in the Hydra/Antlia search area. Hatched areas mark galaxies observed at the SAAO, cross-hatched by others. The top panel gives the number of galaxies while the bottom panel displays the completeness in percent of the total number of galaxies in the deep galaxy search (cf. Fig. 1).

bution of all the 3279 galaxies discovered in the galaxy search (see Fig. 1) – with its various distinct over- and underdensities.

How representative are these galaxies compared to the survey in general? To assess this, we have plotted the magnitude and diameter distribution of the galaxies with redshifts in Fig. 3. In the top panel the number of galaxies with redshifts are displayed, while the bottom panel shows the completeness achieved with respect to the deep galaxy sample in the ZOA in the Hydra/Antlia extension (KK94). The hatched areas are based on the observations at the SAAO, the cross-hatched on others.

The magnitude histogram, combined with the completeness distribution, clearly implies that we can trace the bright end of the magnitude distribution quite well with our observations. Although we have redshifts of 'only' 4% of the deep Hydra/Antlia galaxy survey, we are 92% complete for galaxies brighter than $B_J = 14\overset{m}{.}5$, a typical magnitude limit for complete redshift surveys as, for instance, the first CFA survey (Davis *et al.* 1982), and 70% complete for $B_J = 15\overset{m}{.}5$, the limit for the extended CFA survey (Huchra *et al.* 1994). We are even 50% complete down to $B_J = 16\overset{m}{.}5$.

Although high central surface brightness, and not the apparent B_J-magnitude, is the dominant condition for observations at the SAAO, the histogram in Fig. 3 effectively finds a very steep magnitude cut-off at $B_J = 17\overset{m}{.}3$. Above this magnitude the 1.9m telescope clearly is not sensitive enough to obtain a reasonable spectrum from the galaxies. At the fainter end of our magnitude distribution ($16\overset{m}{.}5 \lesssim B_J \lesssim 17\overset{m}{.}3$), the restriction of high central surface brightness automatically leads to the selection of very compact, face-on small galaxies, the majority of which often are of early type and quite distant (60% with $B_J > 16\overset{m}{.}5$ have $v > 10000\,km\ sec^{-1}$).

The few bright galaxies without redshifts typically are very extended low surface brightness galaxies. This can be deduced indirectly from the diameter distribution which is much broader, nearly gaussian in shape: the distribution does not rise as steeply compared to the magnitude distribution, nor does it have a sharp cut-off for smaller galaxies. The reason is that many of the large galaxies are spirals with an extended large (obscured) low surface brightness disk. They are bright only (apparent magnitude) because of their dimensions. This is evident also from the completeness distribution: we are 'only' 62% complete for $D > 60''$ ($logD = 1.78$), 48% for $D > 45''$ (1.65), but still 35% for $D > 30''$ (1.48). The selection of high surface brightness results in this relatively high fraction of small and compact galaxies and therewith to a much shallower decline of the detections towards smaller galaxies.

As mentioned before, the missing large low surface brightness galaxies ($D > 60''$) have since been observed at Parkes (1993 and 1994). Only few remained undetected. It will be interesting to do follow-up observations of these few extended low surface brightness objects to test whether these are fairly local gas-poor dwarfs.

Altogether it can be maintained that the observed galaxies are representative of the bright end of the luminosity distribution of the galaxies in the Zone of Avoidance. However, it should be stressed again that the above parameters are uncorrected for extinction. The absorption is of the order of 1^{mag} at the borders of our search area, increasing to $5-6^{mag}$ closer to the dust equator. For higher obscuration values the galaxies are obscured away and are

not visible anymore on the IIIaJ, nor on the infrared I sky survey plates of the ESO/SERC.

In the forthcoming catalogue (KK94), the HI-column densities will be listed for each galaxy. This can be used as a rough estimate of the foreground extinction. Together with the formalism of Cameron (1990), we can then correct for the diminishing effects on the diameters and magitudes of the galaxies. This correction will be quite rough and does, of course, not account for the locally varying gas-to-dust ratios. In this first paper on redshift measurements in the ZOA we do not yet attempt any corrections for extinction or an assessment of the completeness of the sample under discussion with regard to the extinction-corrected parameters. We have currently began a program to derive accurate extinction values in the ZOA. A brief outline is given in Kraan-Korteweg *et al.* (1994a). This will be implemented in our final analysis – which will include the data from all observing programs – and discussed there in full detail.

3. Extragalactic structures in the ZOA and its connectivity to structures adjacent to the Milky Way

3.1. The velocity distribution

Fig. 4 shows a histogram of the redshift distribution within the search area. The histogram contains the 115 reliable redshift values of extragalactic objects obtained in this observational program (hatched area) as well as the 31 galaxies in this area with velocities published in the literature (cross-hatched), *i.e.*, it displays the velocity distribution of the galaxies plotted in galactic coordinates in Fig. 2. with the magnitude and diameter distribution as in Fig. 3.

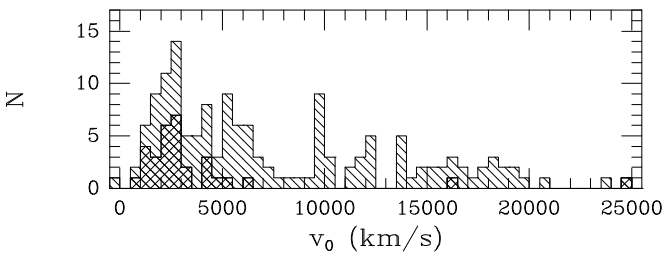

Fig. 4. Velocity histogram of the galaxies in the search area in the Hydra/Antlia extension in the ZOA. Hatched areas are velocities measured by us; cross-hatched by others.

Of the 146 galaxies in total, with redshift measurements there are only three with $v_0 > 20000\,km\ sec^{-1}$, while over two thirds (N=102) have $v_0 < 10000\,km\ sec^{-1}$. Thus we can expect this survey to be useful for tracing structures closer than $10000\,km\ sec^{-1}$, with some indication of structures out to $20000\,km\ sec^{-1}$.

In the nearby velocity range ($v_0 < 10000\,km\ sec^{-1}$), the peaks at 2500, 5000 and $9500\,km\ sec^{-1}$ stand out quite prominently. Are they significant? Are these the first indications of extragalactic structures unveiled in the Southern Milky Way plane? Due to the extreme and locally varying extinction effects in our galaxy sample it is difficult to quantify the significance of these distinct peaks, *i.e.*, to compare the velocity distribution obtained here with the *expected* velocity distribution for a homogenously distributed galaxy sample with well defined selection criteria, such as a diameter, magnitude or velocity completeness limit. Our velocity data is – as discussed in the previous section – almost complete for $B_J \leq 14\overset{m}{.}5$ and decreases gradually in completeness to $\approx 25\%$ at $B_J \approx 17\overset{m}{.}5$. It is quite clear, however, that this distribution is not the result of a homeogenous distribution of galaxies. The peaks in the velocity histogram at 2500, 5000 and $9500\,km\ sec^{-1}$ are too striking and surely originate from individual extragalactic structures such as clusters, filaments and possibly voids. We will therefore now try to localise the features suggested in the histogram here in 3-dimensional space. This can be visualized best by studying the distribution of the observed galaxies in various projections.

3.2. 3-D distribution of the galaxies in the search area and its surroundings

Our sample volume can be projected or "sliced" in various ways, to examine the distribution of the data. Experience has shown that particular structures often show up best in certain favoured directions and not in others. Aside from the data of the present survey, we will also extend the plots to include surrounding regions (similarly as in Fig. 1). The data from the areas adjacent to our survey are taken again from the compilation of the Southern Redshift Catalogue (SRC) by Fairall and Jones (1991) and the 2Jy IRAS Redshift Survey (Strauss *et al.* 1992). They are combined with the velocities obtained here to reveal the connectivity with known structures and/or disclose new ones.

In studying the 3-D distributions in and around our survey region, the reader should be aware of an unavoidable selection effect: the combined data is uncontrolled in magnitude. The true apparent magnitudes of our surveyed galaxies are, as discussed above, very uncertain, due to the irregularities of the foreground extinction. The SRC data is a compilation of published redshifts from all available sources, and does not provide a statistically-controlled sample. Experience has shown though that it contains most of the galaxies with $B_J < 15\overset{m}{.}0$ and $D > 1'$ north of our survey region. South of our sample area, the coverage is less complete, since the sky towards the South Celestial Pole has received less attention. Due to the obscuration of the ZOA, and therefore the fact that most extragalactic studies concentrate on high-latitude region,

the strip $10° < |b| < 20°$ is strongly undersampled in the SRC, while very few SRC redshifts are, of course, found with $|b| < 10°$. This implies that there is as yet hardly any data for the ZOA *on either side of our survey area*.

The absence of magnitude control implies that the density of galaxies projected onto the sky generally does not give a reflection of the true density (for the survey region itself, a detailed discussion of the achieved coverage compared to the deep galaxy search has been presented above). Distinct redshift peaks, however, are completely independent of these selection effects. Extinction effects and variations in limiting magnitude only affect the general decline in galaxy numbers with increasing redshift. They can never preselect towards a particular redshift peak.

The accompanying plots should therfore be interpreted as follows: an elongated feature (a concentration of galaxies in redshift space) that runs radially with the line of sight is suspect. It could be real (a cluster or a filament running outwards), but it could also have been created by a hole in the extinction (in the ZOA), or – in the case of the SRC – a favoured small survey region. An elongated feature that runs across the radial direction has, to be real, however, since it is created by a sequence of distinct redshift peaks over different directions in the sky. A similar argument can be applied to voids (the opposite of a redshift peak): voids have to be real if they are enclosed, on their far side, by a significant number of galaxies. It is possible to establish a statistical measure by means of a technique given in Kauffmann and Fairall (1991), but this is a major undertaking and outside the scope of the present paper.

3.2.1. Sky projections

We begin with sky projections in galactic coordinates. The distributions are *sliced* in redshift intervals of $\Delta v = 2000\,km\ sec^{-1}$ at progressively larger distances, starting at $v = 1000\,km\ sec^{-1}$ in the top left panel, moving downwards and ending at $v = 17000\,km\ sec^{-1}$ at the bottom right panel. Within the individual panels the different symbols give further distance information: the filled dots outline the galaxies within the lower $\Delta = 1000\,km\ sec^{-1}$ velocity interval and the crosses the higher Δv-range. The first slice ($v < 1000\,km\ sec^{-1}$) is not illustrated because it contains only one galaxy. This galaxy (at the surprisingly low latitude of $b = 2.23°$) is discussed in detail under special cases (KK2463).

The first plot (top left) in Fig. 5 clearly shows the Antlia extension as an obvious linear structure descending from top centre of the diagram towards our survey area, so to intersect the Galactic Plane at an angle of about 70°. This panel shows quite clearly that the Hydra and Antlia clusters are not isolated clusters in space but form part of a larger structure – as suspected – that crosses the plane and continues with a concentration of galaxies within our survey area south of the plane. The linear filament is less pronounced there; it seems to break up into two filaments.

In the second plot ($3000 < v_0 < 5000\,km\ sec^{-1}$) the filamentary continuation is hardly visible anymore within our search area. However, due to the velocity dispersion in the cluster itself, Antlia is still distinct, while the Hydra I cluster, and also part of the Centaurus cluster to the left of it, clearly are the dominant features in this panel. A more detailed investigation of the velocity distribution manifests that the Hydra filament starts at a velocity of about $2500\,km\ sec^{-1}$ in the galaxy concentration below the galactic plane, flowing outwards in redshift space to Antlia at about $2800\,km\ sec^{-1}$ and then to Hydra at $\approx 3300\,km\ sec^{-1}$. It is similar to the Puppis filament visible in the top panel, which starts in the GP ($\ell \approx 245°$) at $1500\,km\ sec^{-1}$ and leads to the Antlia cluster as well, from where it possibly continues to the Centaurus cluster.

As discussed above, the data below the southern Milky Way is sparse, but it is not inconceivable that this filamentary Hydra/Antlia extension does continue even further and connects with the Fornax cluster. This link is quite pronounced in the distribution of the extragalactic light (cf. Fig. 2 in Lynden-Bell & Lahav 1988) and has been recognised independently by Mitra (1989). He called it the Southern Supercluster and determined its mean velocity at $1800\,km\ sec^{-1}$.

A second wall, perpendicular to the first (*i.e.*, at about 30° to the plane and mainly north of it), appears in the second plot and possibly persists through to the 5th or 6th plots; it is prominent in the third plot ($5000 < v_0 < 7000\,km\ sec^{-1}$) and its intersection with the first wall there coincides with the Vela overdensity ($\ell \approx 280°, b \approx +6°$).

A surprising result of our spectroscopic data is that the Vela overdensity, which lies exactly in the Antlia extension, is not – as expected – part of this general structure. It is prominent in the third plot, and accounts for the redshift peak at 5000-6000 $km\ sec^{-1}$ in the velocity histogram. The distribution of the other galaxies in this panel is quite surprising as well: although the data coverage is minimal adjacent to our survey region, the majority of the galaxies are found next to this boundary while the remaining region is nearly devoid of galaxies. In the analysis of the redshift slices (see the middle right-hand panel of Fig. 6 and further discussions there) this structure stands out even more conspicuously. It seems a shallow but large-scale overdensity.

Beyond $9000\,km\ sec^{-1}$, a concentration of galaxies south of the plane accounts for the histogram peak at $9500\,km\ sec^{-1}$. The data beyond is sparse, but all four right-hand plots in Fig. 5 show a top-left to bottom-right tendency, with support from the new data in our survey area. The concentration that occurs in the top-left corner is the Shapley region or 'Alpha' region, thought by some (*e.g.*, Vettolani *et al.* 1990) to be the greatest overdensity within $20000\,km\ sec^{-1}$. The concentration in the bottom-

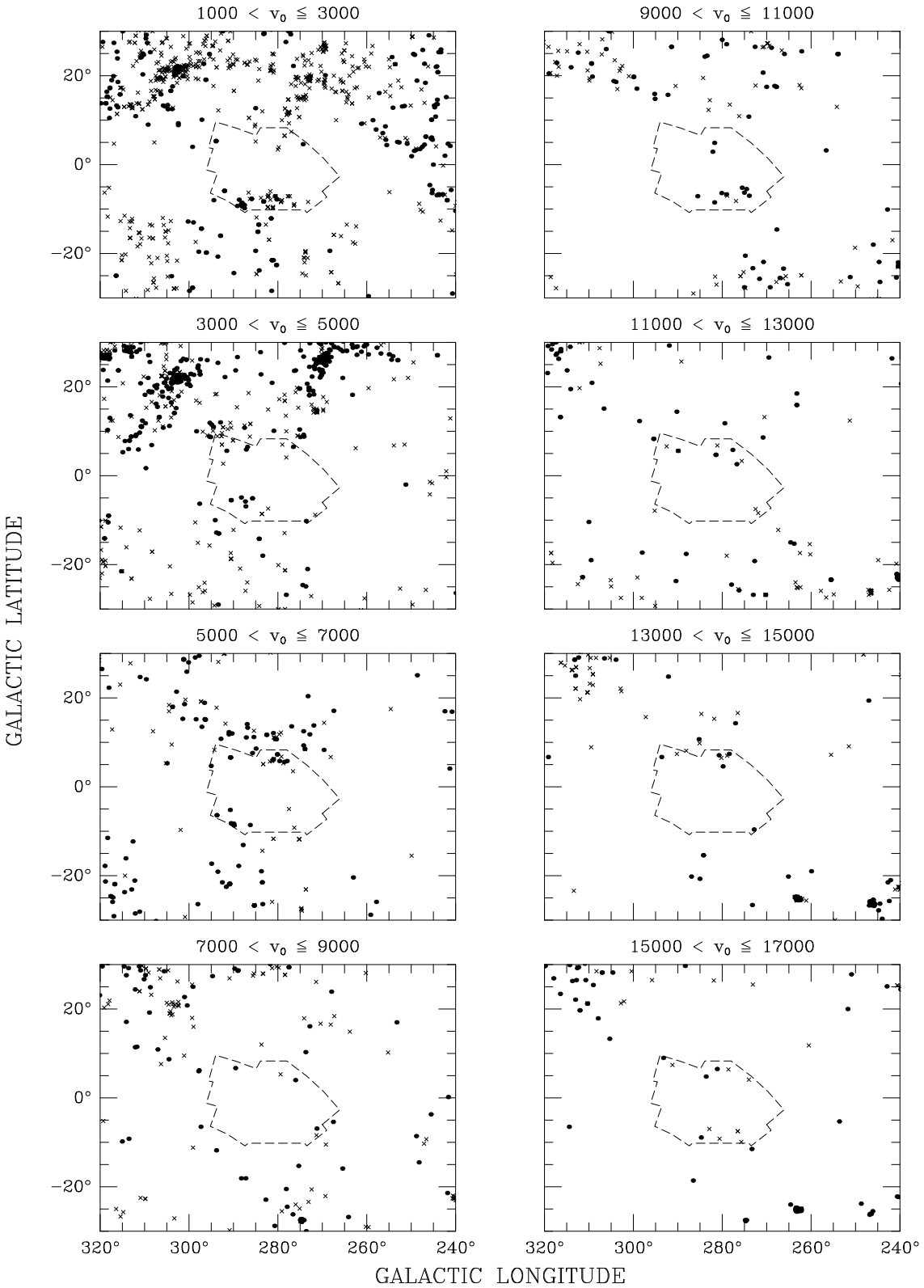

Fig. 5. Sky projections in galactic coordinates for redshift intervals of $\Delta v = 2000\,km\ sec^{-1}$. Within the panels the redshifts are subdivided into intervals of $\Delta v = 1000\,km\ sec^{-1}$: filled dots mark the nearer redshift interval (*e.g.*, $1000 < v_0 \leq 2000\,km\ sec^{-1}$ in the top-left panel), crosses the more distant interval ($2000 < v_0 \leq 3000\,km\ sec^{-1}$ in same panel). The skyplots increase in velocity-distance from the top-left panel to the bottom-right panel as marked above each panel. The area of our investigation is outlined.

right corner (in the 5th to 7th plots) are the Horologium clusters. The Horologium and the Shapley regions dominate the $10000 - 20000\,km\ sec^{-1}$ velocity range.

Note that the data in our sample volume shows a substantial number of galaxies in this redshift range – even more so than outside the Shapley and Horologium regions in the other slices, and despite the fact that our sample volume is lighter sampled than the adjacent regions. Are the Shapley and Horologium regions *one major structure bisected by the Milky Way*? Considering the claims of the significance of the Shapley region, the revelation that it is but a part of an even larger structure is obviously extremely important.

This feature may represent a massive overdensity – its coincidence with the microwave dipole a major gravitational influence on local structures. However, this will only be the case if this structure is singular in its existence. Until we know the distribution of galaxies over the whole sky out to distances beyond this large wall (or sheet), we cannot assess whether this structure is exceptional and whether the gravitational perturbation of its mass is not counterbalanced by similiar structures on opposite parts of the sky. Whatever the case, the size of this structure – if confirmed to be one coherent wall or sheet – will have important cosmological implications: covering about 100° on the sky at a velocity of about $\sim 15000\,km\ sec^{-1}$ it extends over ~ 250 h^{-1} Mpc. This would be the largest structure recognised in the Universe to date, nearly twice the size of the Great Wall.

Obviously, the scarcity of the data at this redshift makes this finding somewhat tentative, but with the addition of our fiber-optic data (in preparation) which will concentrate on the densest areas in the galaxy distribution and probe much deeper ($B_J \approx 19.0 - 19\overset{m}{.}5$) this important structure will be traced in detail. So far, preliminary results from the multifiber spectroscopy indeed support the existence of this large wall (cf. Kraan-Korteweg *et al.* 1993, 1994a).

3.2.2. Redshift slices

We now examine the distribution in conventional 'pie-shaped' redshift slices (wedge diagrams). Fig. 6 shows sequential slices in latitude, *i.e.*, above the ZOA the ($+15° < b \leq +45°$), in the ZOA ($-15° \leq b \leq +15°$) and below the ZOA ($-45° < b \leq -15°$). The panels on the left go out to $v_0 < 5000\,km\ sec^{-1}$ – to trace the Hydat/Antlia extension, the ones on the righthand side out to $v_0 < 10000\,km\ sec^{-1}$ – to outline the Vela overdensity. A slightly larger area of sky is displayed compared to Fig. 5 (the longitude range is $230° < \ell < 330°$). The new data occurs in the central slices in which the broken lines delineates the area investigated here. Filled dots are measurements from the SAAO, crosses from the literature. The slice represent the same features as identified in Fig. 5, but they are now seen at right angles to the previous view.

The uppermost slices (Northern Galactic Hemisphere) show the dominant Centaurus (left) and Antlia plus Hydra I (right) clusters, together with the general concentration of the Centaurus supercluster. The data in the lower slices is sparser, since sampling south of the Galactic Plane and close to the South Celestial Pole is much thinner.

At $v_0 < 3000\,km\ sec^{-1}$, the new data (filled dots in the middle panel) show a sort of filamentary structure, previously referred to as the 'Hydra-Antlia' wall, but which now shows a concentration at $v_0 = 2200\,km\ sec^{-1}$ (the earlier sky plots show this to lie south of the Galactic Plane). This structure represents a continuation of the Hydra-Antlia supercluster downwards through the Galactic plane, and also a connection to the Fornax Wall, in the lowermost plots.

Most of the other new data fill in the region $3000 < v_0 < 6000\,km\ sec^{-1}$, but the points are spread more uniformly (between the broken lines). This is the second wall, described in relation to Fig. 5, but now seen almost flat on - hence the lack of discernable structure.

The galaxy distribution falls off abruptly beyond $v_0 = 7000\,km\ sec^{-1}$ (*cf.*, middle right plot), creating an underdense region up to the perimeter of the diagram (i.e. towards $10000\,km\ sec^{-1}$). Very likely this is caused by the presence of one or more voids. The fact that we find quite a number of galaxies in our survey beyond $10000\,km\ sec^{-1}$ (*cf.*, also Kraan-Korteweg *et al.* 1993, 1994a) emphasizes that the boundary just beyond $7000\,km\ sec^{-1}$ is real and not an artifact.

In this projection the shallow galaxy overdensity around $(\ell, b, V) \approx (280°, +6°, 6000\,km\ sec^{-1})$ – which was first recognised by Kraan-Korteweg and Woudt (1994a) – is even more pronounced. In addition to the points displayed in the middle right plot, it hosts the cluster S0639 (not shown here) at $(\ell, b, V) = (280°, +11°, \sim 6000\,km\ sec^{-1})$ as well. This dense cluster is presently being analysed by Stein (1994). Independent support for the existence of the Vela overdensity, as well as its importance, is given by Hoffman (1994) who applied his density reconstruction algorithm based upon constrained realizations of the density field using Wiener filtering to IRAS-galaxies from the 2Jy Redshift Survey. He predicts a massive overdensity very close to this location and velocity $(285°, +5°, \sim 6000\,km\ sec^{-1})$. It is embedded in a density contour, which contains the Hydra/Antlia/Centaurus overdensity at about $3000\,km\ sec^{-1}$, the Great Attractor density peak at about $4500\,km\ sec^{-1}$ *and* the Vela overdensity at $6000\,km\ sec^{-1}$. The latter is comparable in size and strength to the Hydra/Antlia/Centaurus peak. Earlier reference to the existence of this structure has been given by Saunders *et al.* 1991, who predicted a supercluster (S4) at this location and distance $(281°, +0°, 6120\,km\ sec^{-1})$ – although it was only a 3σ density peak with the data available at that time. The

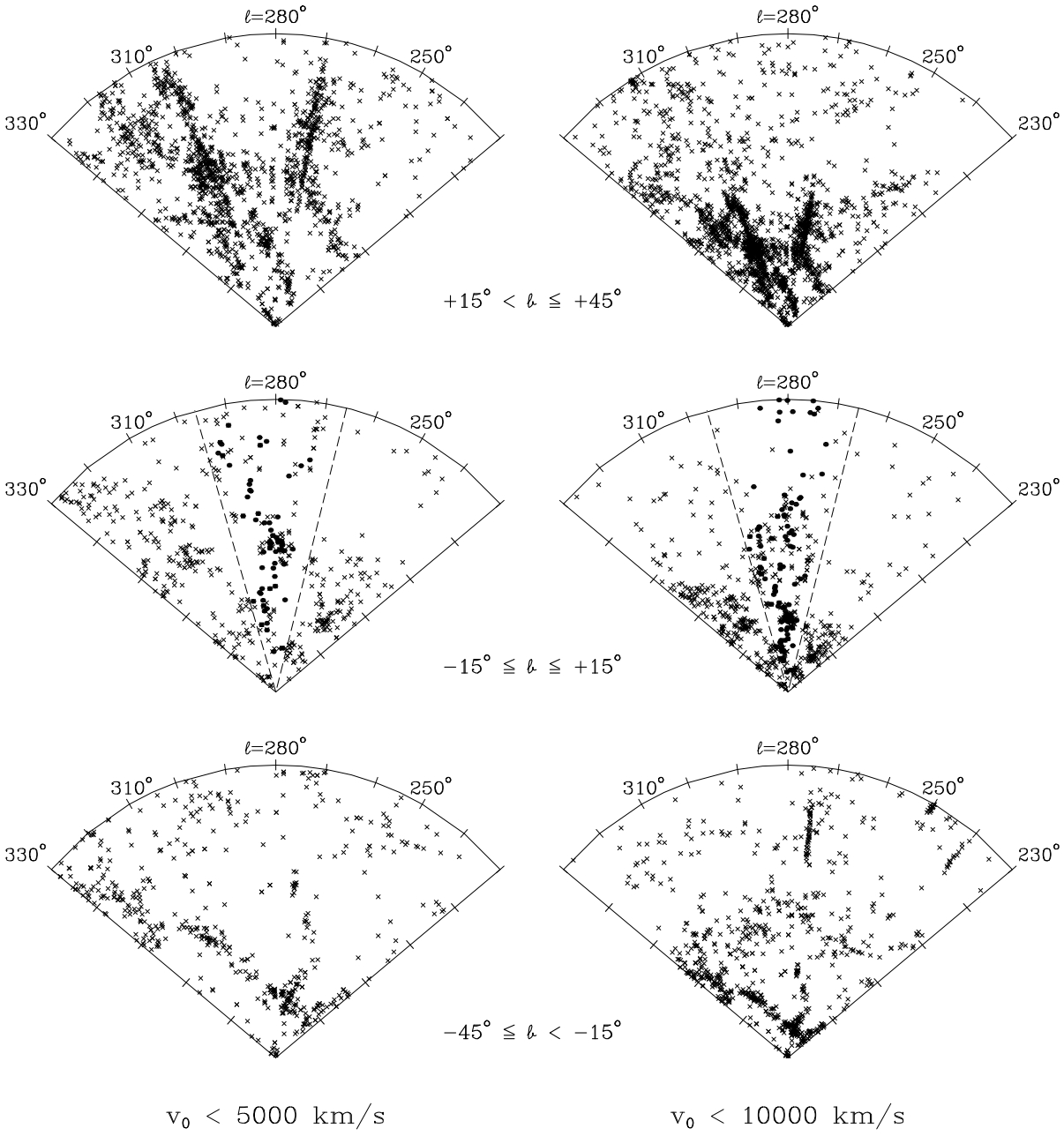

Fig. 6. Redshift slices out to $v_0 < 5000\,km\ sec^{-1}$ (left panel) and $v_0 < 10000\,km\ sec^{-1}$ (right panel) for the longitude range $230^\circ < \ell < 330^\circ$. The top panels display the structures above the GP ($+15^\circ < b \leq +45^\circ$) the middle panel in the GP ($-15^\circ \leq b \leq +15^\circ$) and the bottom panel the structures below the GP ($-45^\circ < b \leq -15^\circ$). The dashed lines in the middle panel delimits the survey area. Filled dots are measurements from the SAAO, crosses from the literature.

close correspondence of these density peaks indicate that they are consistent with one another.

A conspicuous wall runs diagonally downward in the last two slices. This feature was first revealed in wedge diagrams Kraan-Korteweg (1992b) and was previously unrecognised in plots of equatorial coordinates. Projection in rectangular coordinates (Fairall *et al.* 1994) shows it to be an extension of the 'Fornax Wall'.

4. Conclusions

This paper is the first of a series with the aim of tracing the 3-dimensional galaxy distribution in the Southern Milky Way as close as possible to the dust equator. Our basis for these investigations are deep optical galaxy searches done by one of us on sky survey plates. We have presented here 115 new redshifts from optical spectroscopy obtained with the 1.9m telescope of the SAAO.

The SAAO-observations are well suited for observations of the bright end of the luminosity function ($B_J < 17^m.3$) of the deep galaxy search. They are furthermore selected to give homogenous coverage over the whole search area. The results demonstrate that we can trace structures out to 10000 $km\ sec^{-1}$ with indications of structures out to 25000 $km\ sec^{-1}$. The 115 redshifts have been combined with other published velocity data in our search area. The most interesting features uncovered are:

- The earlier suspected Hydra/Antlia extension across the Milky Way could be confirmed. It can be traced from the Hydra I cluster at $\ell = 270°, b = 28°, v \sim 3300\,km\ sec^{-1}$ towards the here unveiled group at $280°, -7°, \sim 2500\,km\ sec^{-1}$. It seems more a filamentary structure, consisting of spiral-rich groups and clusters, rather than a supercluster. The Hydra/Antlia filament will be bring the dipole direction as derived from accumulation of the gravitational forces of galaxies in better agreement to the CMB measurement. It is possible that this filament continues and extends to the Fornax cluster ($240°, -57°, \sim 1450\,km\ sec^{-1}$).
- The prominent galaxy overdensity in Vela is part of previously unrecognised shallow, large-scale, overdensity centered on $\sim 6000\,km\ sec^{-1}$. The independent predictions of a supercluster in the ZOA at this positon and distance by Hoffman (1994) and Saunders *et al.* (1991) indicate that it could be quite a massive.
- The distribution of the distant galaxies seem to bridge the Shapley concentration and the Horologium clusters. If substantiated with our forthcoming data, this wall/sheetlike feature of about 250 h^{-1}Mpc will be the largest coherent structure detected in the Universe, its large size difficult to reconcile with current cosmological models.

As this is the first paper on our redshift observations, discussions on the achieved completeness of the observed sample - which is not straightforward to assess through the murk of the Milky Way plane – has not been attempted.

Acknowledgements. The authors would like to thank the night assistants Francois van Wyk and Frans Marang as well as the staff at the SAAO for their hospitality. The research by RCKK has been made possible by a fellowship of the Royal Netherlands Academy of Arts and Sciences. Support was also provided by CNRS through the Cosmology GDR program.

References

Aaronson, M., Huchra, J., Mould, J., et al., 1982, ApJ 258, 64
Acker, A., Stenholm. B., Veron, P. 1991, AASS 87, 499
Burstein, D., Heiles, C. 1982, AJ 87, 1165
Cameron, L.M. 1990, A&A 233, 16
4^{th} DAEC Meeting on "Unveiling Large-Scale Structures behind the Milky Way", eds. C. Balkowski and R.C. Kraan-Korteweg, ASP Conf. Ser., in press
Corwin, H.G. Vuacouleurs, A.de, Vaucouleurs, G. de 1985, Southern Galaxy Catalogue, Univ. Texas Monographs in Astron. No. 4, Austin: Univ. of Texas
Davis, M., Huchra, J.P., Latham, D.W., et al., 1982, ApJ 253, 423
Dekel, A. 1994, ARAA, in press
Dressler, A. 1991, ApJS 75, 241
Dressler, A., Faber, S.M. 1990a, ApJ 354, 13
Dressler, A., Faber, S.M. 1990b, ApJL 354, L45
Fairall, A.P., Paverd, W.R., Ashley, R.P. 1994, in 4^{th} DAEC Meeting on "Unveiling Large-Scale Structures behind the Milky Way", eds. C. Balkowski and R.C. Kraan-Korteweg, ASP Conf. Ser., in press
Fairall, A.P., Jones, A. 1991, Southern Redshifts Catalogue and Plots, Publ. Dept. Astr., Univ. Cape Town, No. 11.
Hoffman, Y. 1994, in 9^{th} IAP Astrophysics Meeting and 3^{rd} Meeting of the EARA on "Cosmic Velocity Fields", eds. F. Bouchet and M. Lachièze-Rey, Editions Frontieres, Gif-sur-Yvette, 357
Huchra, J.P., Vogeley, M.S., Geller, M.J. 1994, in prep.
Huchtmeier, W.K. Richter, O.-G., 1989, The General Catalogue of HI-Observations of Galaxies, New York: Springer-Verlag
Hudson, M. 1993, MNRAS 265, 72
Hudson, M. 1994, MNRAS 266, 475
Jerjen, H., Tammann, G.A. 1993, A&A 276, 1
Jordon, A.R., Read, P.D., van Breda, I. 1982, SPIE Conference "Instrumentation in Astronomy IV", Tucson
Kauffmann, G., Fairall, A.P. 1991, MNRAS 248, 313
Kerr, F.J., Bowers, P.F., Jackson, P. D., et al., 1986, A&AS 66, 373
Kogut, A., Lineweaver, C., Smoot, G.F., et al., 1993, ApJ 419, 1
Kolatt, T., Dekel, A., Lahav, O. 1994, MNRAS, in press
Kraan-Korteweg, R.C. 1989, in Reviews in Modern Astronomy 2, ed. G. Klare, Springer: Berlin, 119
Kraan-Korteweg, R.C. 1991, in Workshop on Large-Scale Structures and Peculiar Motions in the Universe, eds. D.W. Latham and L.N. daCosta, ASP Conf. Ser., 165
Kraan-Korteweg, R.C. 1992a, in 2^{nd} DAEC Meeting on The Distribution of Matter in the Universe, eds. G. Mamon and D. Gerbal, Observatoire de Paris Press: Paris, 202
Kraan-Korteweg, R.C. 1992b, in Variable Stars and Galaxies, Symp. in honour of M.W. Feast, ed. B. Warner, ASP Conf. Ser., 235
Kraan-Korteweg, R.C. 1994, in preparation [KK94]
Kraan-Korteweg, R.C., Fairall, A.P., Balkowski, C., et al., 1993, in International Meeting on "Observational Cosmology", eds. G. Chincarini et al., ASP Conf. Ser., 106
Kraan-Korteweg, R.C., Cayatte, V., Fairall, A.P., et al., 1994a, in 4^{th} DAEC Meeting on "Unveiling Large-Scale Structures behind the Milky Way", eds. C. Balkowski and R.C. Kraan-Korteweg, ASP Conf. Ser., in press
Kraan-Korteweg, R.C., Fairall, A.P., Woudt, P.A., et al., 1994b, in prep.
Kraan-Korteweg, R.C., Huchtmeier, W.K. 1992, A&A 266, 150
Kraan-Korteweg, R.C., Woudt, P. 1994a, in 9^{th} IAP Astrophysics Meeting and 3^{rd} Meeting of the EARA on "Cosmic Velocity Fields", eds. F. Bouchet and M. Lachièze-Rey, Editions Frontieres, Gif-sur-Yvette, 557
Kraan-Korteweg, R.C., Woudt, P. 1994b, in 4^{th} DAEC Meeting on "Unveiling Large-Scale Structures behind the Milky Way", eds. C. Balkowski and R.C. Kraan-Korteweg, ASP Conf. Ser., in press

Lahav, O., Yamada, T., Scharf, C., et al., 1993, MNRAS 262, 711-716
Lauberts,A. 1982, The ESO/Uppsala Survey of the ESO (B) Atlas, ESO: Garching
Lauer, T.R., Postman, M. 1993, in Observational Cosmology, eds. G. Chincarini *et al.*, ASP Conf. Ser. 51, 171
Lu, N.Y., Dow, M.W., Houck, J.R., et al., 1990, ApJ 357, 388
Lynden-Bell, D., Faber, S.M., Burstein, D., et al., 1988, ApJ 326, 19
Lynden-Bell, D., Lahav, O. 1988, in Large-Scale Motions in the Universe, Proc. of the Vatican Study Week, eds. G. Coyne & V.C. Rubin, Princeton University Press, Princeton
Lynden-Bell, D. Lahav, O., Burstein, D. 1989 MNRAS 241, 325
Mathewson, D.S., Ford, V.L., Buchhorn, M., 1992, ApJ 389, L5
Meurs, E.J.A. and Harmon, R.T. 1988, A&A 206, 53
Mitra, S. 1989, AJ 98, 1175
Plionis, M., Coles, P., Catelan, P. 1993, MNRAS 262,465
Rowan-Robinson, M., Lawrence, A., Saunders. W., et al., 1990, MNRAS 247, 1
Sandage, A., Tammann, G.A. 1981, A Revised Shapley-Ames Catalog of Bright Galaxies (RSA), Washington DC: Carnegie Institution of Washington)
Saunders, W., Frenk, C., Rowan-Robinson, M., et al., 1991, Nature, 349, 32
Scaramella, R., Vettolani, G., Zamorani, G. 1991, ApJL 376, L1
Scharf, C., Hoffman, Y., Lahav, O., et al.,1992, MNRAS 256, 229
Stein, P. 1994, Ph.D. thesis, Univ. of Basel, in prep.
Strauss, M.A., Yahil, A., Davis, M., et al., 1992, ApJ 280, 470
Tammann, G.A., Sandage, A. 1985, ApJ 294, 81
Vaucouleurs, G. de, Vaucouleurs, A. de, Corwin, H.G. 1976, Second Reference Catalogue of Bright Galaxies (RC2), University of Texas Press, Austin
Vettolani, G.P., Chincarini, G., Scaramella, R., et al., 1990, AJ 99, 1709

This article was processed by the author using Springer-Verlag LaTeX A&A style file *L-AA* version 3.